

Numerical reconstruction of pulsatile blood flow 4D computer tomography data

Attila Lovas^{a,*}, Róbert Nagy^c, Elek Csobo^a, Brigitta Szilágyi^b,
Csaba Csobay–Novák^d, Péter Sótonyi^d

^a Budapest University of Technology and Economics, Department of Analysis, Building H,
Egry József str. 1, Budapest, Hungary 1111

^b Budapest University of Technology and Economics, Department of Geometry, Building H,
Egry József str. 1, Budapest, Hungary 1111

^c Budapest University of Technology and Economics, Department of Structural Mechanics,
Building K, Műegyetem rkp. 3, Budapest, Hungary 1111

^d Semmelweis University, Heart and Vascular Center, Department of Vascular Surgery,
Városmajor str. 68, Budapest, Hungary 1122

Abstract

We present a novel numerical algorithm developed to reconstruct pulsatile blood flow from ECG-gated CT angiography data. A block-based optimization method was constructed to solve the inverse problem corresponding to the Riccati-type ordinary differential equation that can be deduced from conservation principles and Hook's law. Local flow rate for 5 patients was computed in 10 cm long aorta segments that are located 1 cm below the heart. The shapes of the local flow rate curves seem to be very realistic. Our approach is suitable for estimating characteristics of pulsatile blood flow in aorta based on ECG gated CT scan thereby contributing to more accurate description of several cardiovascular lesions.

Keywords: biofluid mechanics, pulsatile flow, inverse problem, periodic Riccati equation

2010 MSC: 65M32, 65K10, 76Z05, 92C10, 92C50

1. Introduction

Pulsatile flow in blood vessels has been studied for more than 300 years. Leonard Euler initiated the theory of pressure wave propagation in vascular system in 1775. The first modern mathematical model of pulsatile flow in blood
5 vessels was developed by Diederik Johannes Korteweg and Horace Lamb. Hitherto, numerous attempts have been made to study blood flow in the vascular system. Yunlong Huo and Ghassan S. Kassab have published a Whomersley-type mathematical model to analyze pulsatile blood flow in the entire coronary

*Corresponding author

Email address: lovas@math.bme.hu (Attila Lovas)

arterial tree [1]. Mostly stenosed geometries were investigated owing to their
 10 connection to vascular diseases such as arteriosclerosis which may lead to heart
 attack and stroke [2]. Mir Golam Rabby et al. have investigated numerically
 the effects of non-Newtonian modeling on unsteady periodic flows in a two-
 dimensional pipe with idealized stenoses [3]. In the above mentioned studies,
 motions of the vessel wall were not taken into consideration.

15 ECG-gated computer tomography along with an image segmentation algo-
 rithm based on Active Contour Model [4] enables us to measure the local cross
 sectional area of the vessel as a function of time and the position of the con-
 sidered cross section along the vessel's axis. The main objective of the present
 work is to develop a numerical procedure to compute volumetric flow rate of
 20 blood through the local cross sections of the vessel from the local cross sectional
 area. We assume that there exist a short segment of the vessel where it is thin
 and elastic. Furthermore, the change in the local cross sectional area must be
 caused by the change in blood pressure only, and gravitation has no effect on
 the fluid because the patient is lying during the medical examination. By ap-
 25 plying the one-dimensional Euler momentum equation, equation of continuity
 and Hook's law, we deduced a Riccati-type ODE for volumetric flow rate at the
 beginning of the considered vessel segment closer to the heart. The only periodic
 solution with positive integral was accepted as physically admissible. Existence
 of such a solution can be tested numerically. However, the Riccati-type ODE
 30 contains an extra scalar parameter and can be solved just for fixed parameter
 values. To find the volumetric flow rate a block-based optimization method was
 implemented.

2. Material and methods

2.1. ECG-gated CT angiography

35 Imaging of a pulsatile organ is a highly demanding application for any cross
 sectional imaging modality. Computed tomography (CT) imaging of the heart
 became widely available with the introduction of multi-detector CT (MDCT)
 scanners with four-slice detector arrays and 500 ms minimum rotation time [5].
 Still images of the moving heart was generated using retrospective ECG-gating:
 40 slow table motion during spiral scanning and simultaneous acquisition of the
 slices and the digital ECG trace provided oversampling of scan projections [5].
 After the exposure, slices recorded in the same phase of the ECG trace are
 matched to generate a 3D dataset of the volume of interest, representing ei-
 ther systole or diastole. A drawback of this method is the higher radiation
 45 dose compared to the normal non-oversampled spiral acquisition [6]. An im-
 portant advantage is the possibility to reconstruct multiphasic datasets of the
 same volume, resulting in motion images of the same slices. This allows us the
 functional analysis of the moving organs such as the heart or the great vessels.
 Recent advances in CT technology (256 – 320 detector rows, 270 ms minimum
 50 rotation time) allow for rapid ECG-gated CTA of the whole aorta during a
 single breath-hold.

Imaging of the aorta was performed in 5 patients (5 men, mean age 68.2 ± 6.1 years) with a 256-slice MDCT (Philips Brilliance iCT, Koninklijke Philips N.V., Best, The Netherlands) using a retrospectively ECG-gated protocol tailored for the imaging of the aorta. Investigations were performed on images readily available from patients with suspected aortic disease. Low-dose (tube voltage: 100 kV) native scan was followed by a retrospective ECG-gated CT angiography of the whole aorta (100 kV) with a reduced field of view to maximize spatial resolution. Nonionic contrast agent was injected into an antecubital vein at a flow rate of 4 – 5 ml/s using a power injector. Images were reconstructed using a sharp convolution kernel and iterative reconstruction algorithm (iDose4, Koninklijke Philips N.V., Best, The Netherlands) with a slice thickness of 1 mm and an increment of 1 mm. Multiphase images were reconstructed corresponding every 10% of the R-R cycle resulting in ten series of images for each patient. Patients gave written informed consent before CT examination was performed. Experimental protocol and informed consent was approved by the Regional Ethical Committee of Semmelweis University (133/2011).

2.2. Image segmentation

The first problem which we have to solve in order to compute cross sectional area of the blood vessel is to locate it in the dicom image. This can be carried out by some sort of image segmentation algorithm. In our case, Active Contour Model (ACM) was applied to perform segmentation. The first version of ACM was published by Michael Kass, Andrew Witkin and Demetri Terzopoulos [4] at the end of the 80s.

Active contours are energy minimizing splines in 2D which they are commonly referred to as snakes. It is possible to generalize the algorithm to higher dimensions using energy minimizing surfaces but the corresponding numerical method is usually not stable because a surface might intersect itself or change its topology. For that reason, an algorithm based on a sequential two-dimensional balloon snake model was applied to each phases which means that the final position of the moving snake on a slice was implemented as initial condition on the next one. As the result of the segmentation process, we get the coordinates of the vessel's internal wall for each slices perpendicular to z axis in the region of interest and for all phases in time. For more information about the Active Contours we refer the reader to [7] and [8].

To mitigate the spatial measurement error, we fitted a bicubic smoothing spline to the point cloud resulting from the active contour method in each time step. This way the increase of temporal resolution also became possible exploiting the affine covariance of B-splines and ensuring the periodic movement of the control points by trigonometric approximation using the first 3 harmonics of the heart rate [9]. The cross-sectional area is defined as the area of the section perpendicular to the center line of the fitted surface.

2.3. Governing Equations

To make our exposition self-contained we present some laws of continuum mechanics, these are the conservation laws for mass and momentum. In addi-

tion, empirical constitutive laws are needed to relate certain unknown variables such as relations between stress and strain.

Let us examine the pulsating flow of blood in an artery assuming that the wall is thin and elastic. Owing to the pressure gradient the artery wall deforms and the elastic restoring force of the wall makes it possible for waves to propagate and so it maintains a pulsating motion of the artery. The artery radius $r(t, x)$ varies in time along the artery. Let the local cross sectional area be $S = \pi r^2$ and the averaged flow velocity $u(t, x)$ are periodic in the first argument with period T where T denotes the period of the cardiac cycle. We define the volume flow rate as $q = uS$. Assuming that blood is homogeneous and incompressible we obtain from the law for conservation of mass that

$$\frac{\partial S}{\partial t} + \frac{\partial q}{\partial x} = 0. \quad (1)$$

Additionally the law for conservation of momentum can be written as follows:

$$\frac{\partial u}{\partial t} + u \frac{\partial u}{\partial x} = -\frac{1}{\rho} \frac{\partial p}{\partial x}. \quad (2)$$

We use Hook's law to relate stress and strain rates. Let h be the vessel wall thickness, assumed to be much smaller than the vessel radius, and Young's modulus will be denoted by E . The change in tube radius must be caused by the blood pressure. The elastic strain due to the lengthening of the circumference is dr/r . The change is elastic force must be balanced by the changing in pressure force $2adp$, which implies

$$\frac{dp}{dr} = Ehr^2 \quad \text{and} \quad \frac{dp}{dS} = \frac{\sqrt{\pi} Eh}{2S^{3/2}}.$$

From this we obtain the following:

$$\frac{\partial p}{\partial x} = \frac{hE\sqrt{\pi}}{2S^{3/2}} \frac{\partial S}{\partial x}. \quad (3)$$

3. Calculation

3.1. Periodic Riccati equation

Let us consider a nonbranching cylindral blood vessel segment of length L where equations (1), (2) and (3) are satisfied. If we substitute (3) into (2) we have

$$\frac{\partial u}{\partial t} + u \frac{\partial u}{\partial x} = -\frac{\alpha}{S\sqrt{S}} \frac{\partial S}{\partial x}, \quad (4)$$

where $\alpha = 0.5hE\sqrt{\pi}/\rho$ is assumed to be constant during the cardiac cycle.

If we multiply the left-hand side of (4) by S , using $q = uS$ and integrating by parts we obtain

$$\begin{aligned} \int_0^L S \frac{\partial u}{\partial t} + q \frac{\partial u}{\partial x} dx &= \left[\frac{q^2(t, x)}{S(t, x)} \right]_{x=0}^{x=L} + \int_0^L S \frac{\partial u}{\partial t} + u \frac{\partial S}{\partial t} dx \\ &= \left[\frac{q^2(t, x)}{S(t, x)} \right]_{x=0}^{x=L} + \int_0^L \frac{\partial q}{\partial t} dx. \end{aligned} \quad (5)$$

By applying (1), the volumetric flow rate can be written as

$$q(t, x) = Q(t) + \Phi(t, x), \quad (6)$$

where $Q(t) = q(t, 0)$ and

$$\Phi(t, x) = - \int_0^x \frac{\partial S}{\partial t}(t, y) dy.$$

From this we obtain the following Riccati-type ordinary differential equation

$$\frac{dQ}{dt} = AQ^2 + BQ + C, \quad (7)$$

where coefficients are periodic with period T and can be written as follows:

$$A(t) = -\frac{1}{L} \left[\frac{1}{S(t, x)} \right]_{x=0}^{x=L} \quad (8)$$

$$B(t) = -\frac{2}{L} \frac{\Phi(t, L)}{S(t, L)} \quad (9)$$

$$C(t) = -\frac{1}{L} \left(\frac{\Phi(t, L)^2}{S(t, L)} - 2\alpha \left[\sqrt{S(t, x)} \right]_{x=0}^{x=L} + \int_0^L \frac{\partial \Phi}{\partial t} dx \right). \quad (10)$$

3.2. Periodic solutions

Physically admissible solutions. Assume that $x = 0$ corresponds to the beginning of the considered vessel segment closer to the heart.

Definition 1. A solution of (7) Q is said to be *physically admissible* if it satisfies the following conditions:

- i. $Q : \mathbb{R} \rightarrow \mathbb{R}$ is a periodic function with period T ,
- ii. $\int_0^T Q(t) dt > 0$.

It is well known that the general solution of a scalar Riccati equation can be obtained by quadrature whenever at least one particular solution Q_0 is known. The substitution

$$Q = Q_0 - \frac{1}{W} \quad (11)$$

in the Riccati equation yields

$$\frac{dW}{dt} = -(2Q_0A + B)W + A, \quad (12)$$

which is first order inhomogeneous linear ODE and its general solution can be written as

$$W(t) = KW_h(t) + W_{ih}(t), \quad (13)$$

where W_h is the solution of the homogeneous equation for which $W_h(0) = 1$ holds and W_{ih} is the solution of the inhomogeneous equation for which $W_{ih}(0) = 0$ holds. Periodicity of Q requires that $Q(0) = Q(T)$ that holds if and only if K solves the quadratic equation

$$Q_0(T)K^2 + \left(Q_0(T)\frac{W_{ih}(T)}{W_h(T)} - \frac{W_h(T) - 1}{W_h(T)}\right)K - \frac{W_{ih}(T)}{W_h(T)} = 0, \quad (14)$$

where $Q_0(0)$ is supposed to be zero. The number of periodic solutions depends on the sign of the discriminant that can be tested numerically.

$$\Delta = \left(Q_0(T)\frac{W_{ih}(T)}{W_h(T)} - \frac{W_h(T) - 1}{W_h(T)}\right)^2 + 4Q_0(T)\frac{W_{ih}(T)}{W_h(T)} \quad (15)$$

Although the non-negativity of Δ guarantees the existence of periodic solution, it does not imply that at least one of the solutions is physically admissible.

125 Leon Kotin demonstrated the existence and uniqueness of a positive and of a negative periodic solution of a periodic Riccati equation in which the coefficients satisfy certain general condition. Moreover, any solution which is everywhere continuous lies between these two solutions, and every solution is asymptotic to one of these as the independent variable increases or decreases [10]. More
130 precisely the following is true.

Theorem 1 (Kotin 1968). *If A', B, C in (7) are continuous everywhere and $-AC > 0$ holds, then equation (7) has a unique positive solution Q_+ and a unique negative solution Q_- which are periodic with period T and any solution behaves asymptotically like Q_+ or Q_- as $t \rightarrow \infty$.*

135 *Asymptotic stability.* It is clear that if conditions of Kotin's theorem are satisfied, then Q_+ is the unique physically admissible solution. However, Q_+ may not be asymptotically stable. Consider the case when $C < 0$ and Q is an arbitrary perturbation of Q_+ . From the unicity of the positive solution, we have that there exists $t_0 \in \mathbb{R}$ where Q vanishes and Q can have only one root, since
140 at $Q = 0$ the right-hand side of (7) is equal to C which is negative. As a consequence, we have that the physically admissible solution is not necessarily asymptotically stable.

3.3. Numerical Procedure

The block-based optimization method. For any fixed values of α , the functions W_h and W_{ih} are computed numerically. In cases where $\Delta \geq 0$, periodic solutions of (7) can be expressed as follows

$$Q_{1,2}(t) = Q_0(t) - \frac{1}{K_{1,2}W_h(t) + W_{ih}(t)},$$

where K_1 and K_2 are solutions of (14). In our case, α is not known thus the problem is underdetermined up to a constant. To find the local flow rate further conditions are needed.

To overcome this problem, we consider a second non-branching vessel segment of length L that is adjacent to the previous one such that the end of the first segment is joined to the beginning of the second one. Quantities corresponding to the second vessel segment are denoted by tilded symbols (e.g. \tilde{q} and \tilde{Q}) and α is incorporated as a subscript to indicate the dependence of the considered quantity on the model parameter. We define the so-called "internal consistency" functional

$$I(\alpha) = \int_0^T (\tilde{q}_\alpha(t, 0) - q_\alpha(t, L))^2 dt \quad (16)$$

that measures the mean squared difference between the local flow rate at the beginning of the second vessel segment computed from motions of the second vessel segment and the local flow rate at the end of the first vessel segment calculated from data corresponding to the first vessel segment. The domain of I is

$$\text{dom}(I) = \left\{ \alpha \in \mathbb{R}^+ \mid \Delta_\alpha \geq 0 \text{ \& } \tilde{\Delta}_\alpha \geq 0 \right\}.$$

Let us define the average flow rate corresponding to α by

$$\bar{q}_\alpha = \frac{1}{2T} \int_0^T \tilde{q}_\alpha(t, 0) + q_\alpha(t, L) dt.$$

Our goal is to minimize $I(\alpha)$ for α -s that satisfy $\bar{q}_{min} \leq \bar{q}_\alpha \leq \bar{q}_{max}$, where q_{min} and q_{max} are the minimal and maximal average flow rate which may occur under physiological circumstances.

Sensitivity analysis. At this point we examine the effect of small perturbations of α around the optimal value (α_{opt}). We can write

$$C = C_0 + \alpha C_1, \quad (17)$$

where C_0 and C_1 do not depend on α . First-order approximation of Q_α can be written as

$$Q_\alpha(t) = Q_{\alpha_{opt}}(t) + P(t)(\alpha - \alpha_{opt}) + \mathcal{O}(|\alpha - \alpha_{opt}|^2), \quad (18)$$

where P is called sensitivity coefficient and it is the unique periodic solution of the following first-order linear differential equation:

$$\frac{dP}{dt} = (2AQ_{\alpha_{opt}} + B)P + C_1. \quad (19)$$

150 4. Results

4.1. Local flow rates

Gender, age, body mass index (BMI), heart rate (HR) and dose length product (DLP) are presented in Table 1. Calculations were performed on 10 cm long non-branching segments of the descending aorta. Considered vessel segments
155 are located 1 cm below the heart. In each cases, the last 2×1 cm long parts of the vessel segment provides input data for the block-based optimization algorithm. According to the physiological fact that the cardiac output lies between $4 \text{ dm}^3/\text{min}$ and $6 \text{ dm}^3/\text{min}$, maximal average flow rate (\bar{q}_{max}) was set to $100 \text{ cm}^3/\text{s}$ and the minimal average flow rate (\bar{q}_{min}) to $66.7 \text{ cm}^3/\text{s}$. MATLAB's
160 ode45 function was used to solve differential equations that may occur in simulations.

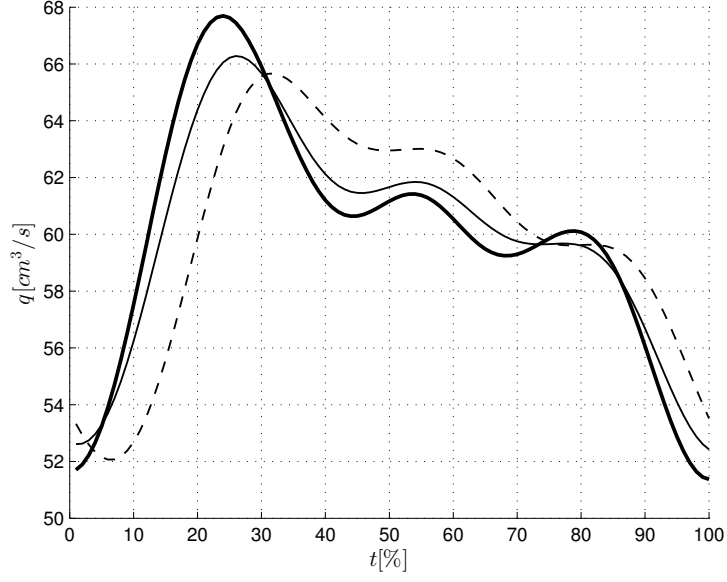
No.	Gender	Age	BMI	HR	DLP
1.	M	69	29.1	60	3504
2.	M	67	23.9	52	2690
3.	M	62	28.9	86	2756
4.	M	65	19.3	59	2161
5.	M	78	24.7	67	2300

Table 1: Patient data. Gender – male (M)/female (F), Age (years), BMI (kg/m^2), HR (bpm), DLP (mGycm).

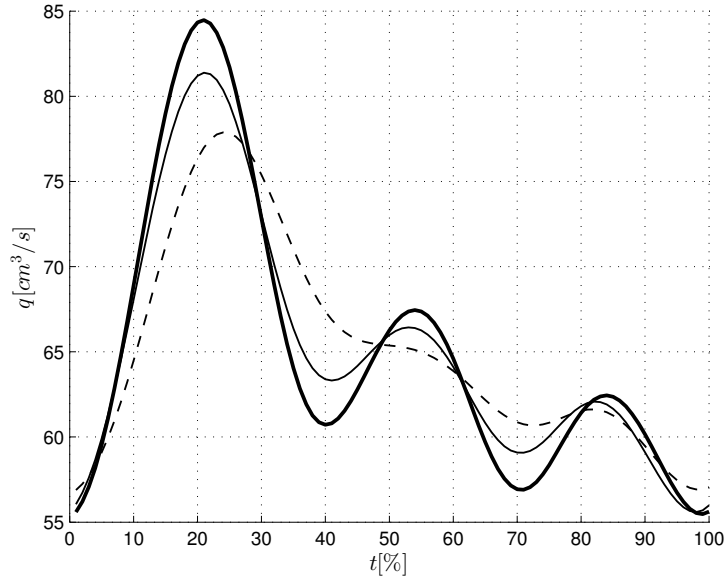
MATLAB's fzero function was applied to compute α values corresponding to the minimal and maximal flow rate. These are α_{min} and α_{max} respectively. We found that iterations converged to a limit in all cases. Global minimum of $I(\alpha)$
165 was computed on the interval $(\alpha_{min}, \alpha_{max})$ by MATLAB's fminbnd function. We found that iterations converged to a minimum in all cases and the interval $(\alpha_{min}, \alpha_{max})$ is a subset of the domain of I that is the feasible set of the optimization problem. Values of α_{min} , α_{max} and α_{opt} in $10^3 \text{ cm}^3/\text{s}^2$ are presented in Table 2. The mean squared error between blocks $\text{MSE} = (I(\alpha_{opt})/T)^{1/2}$
170 is introduced to measure the goodness of the model (Table 2). Conditions of Kotin's theorem were tested and the results are presented in Table 2.

Detailed results are presented for the youngest (patient No. 3) and for the oldest patient (patient No. 5). Local flow rates were calculated at the 10%, 50% and 90% of the aorta segment. We plot the local flow rates corresponding to
175 the youngest and the oldest patient at different equally distributed times during the cardiac cycle in Fig. 1a and Fig. 1b).

We have seen that conditions of Kotin's theorem are satisfied in almost all cases and the only exception is just patient No. 5 who was the oldest person.



(a) Patient No. 3



(b) Patient No. 5

Figure 1: Local flow rate (cm^3/s) in time (% of the cardiac cycle). Thick line – 10%, solid line – 50% dashed line – 90% of the aorta segment.

No.	α_{\min}	α_{\max}	α_{opt}	MSE	Kotin
1.	2.72	7.56	2.75	2.25	+
2.	2.47	6.87	2.47	3.42	+
3.	2.67	7.42	2.68	3.82	+
4.	2.81	7.99	2.88	3.06	+
5.	5.81	15.8	6.82	2.12	-

Table 2: Parameter values corresponding to the minimal, maximal and the optimal local flow rate ($10^3 \text{ cm}^3/\text{s}^2$), MSE (cm^3/s), and conditions of Kotin’s theorem – satisfied (+)/ not satisfied (-).

The typical behaviour of the solutions can be seen in Fig. 2a and the phase picture corresponding to the only non-typical case is illustrated in Fig. 2b.

The graph of the sensitivity coefficients can be seen in Fig. 3a and Fig. 3b.

4.2. Reynolds and Womersley numbers

For the sake of completeness, we give the definitions of Reynolds (Re) and Womersley (Wh) numbers. The first is a dimensionless number in fluid mechanics that is defined as the ratio of inertia forces to viscous forces, expressed in tubular flows as

$$\text{Re} = \frac{2vr\rho}{\eta}, \quad (20)$$

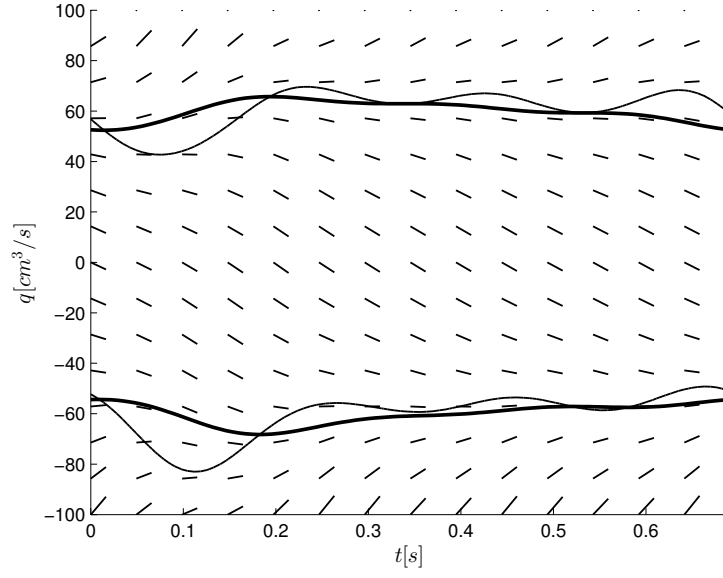
where v is the flow velocity, r is the vessel’s radius, ρ is the blood density and η is the dynamical viscosity of blood. The second is a dimensionless number in biofluid mechanics that relates the transient inertial forces to viscous effects. The Womersley number is defined by

$$\text{Wh} = 2r\sqrt{\frac{\omega\rho}{\eta}}, \quad (21)$$

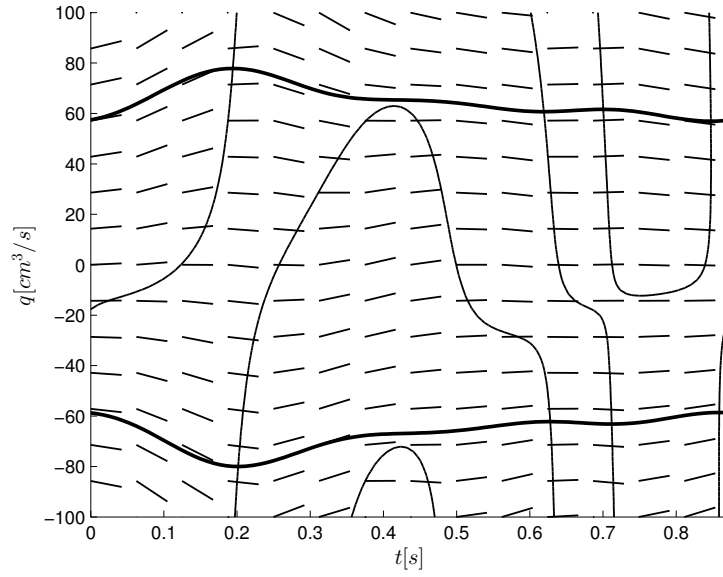
where ω is the angular frequency of the oscillations. In accordance with the literature [11], [12], in our calculations blood density was set to 1.06 g/cm^3 and the kinematical viscosity of blood to $3.5 \times 10^{-3} \text{ Pa} \cdot \text{s}$. Estimatoins for Reynolds and Womersley numbers along the artery segment are illustrated in common coordinate system in Fig. 4a and Fig. 4b.

The Womersley number is a dynamic similarity measure of oscillatory flows relating inertia and viscous forces. In rigid pipes for laminar incompressible flows small values (approx. $\text{Wo} < 1$) allow the development of the parabolic velocity profile of the steady state solution and the flow is almost in phase with the pressure gradient, while large values (approx. $\text{Wo} > 10$) indicate a flat velocity profile with a good approximation and the flow follows the pressure gradient by about 90 degrees in phase. In the presented examples – as seen in Fig. 4a and 4b – the values lie inbetween, yielding a complex time-dependent velocity profile.

The Reynolds number is another dynamic similarity measure relating inertia and viscous forces. In rigid pipes small values (approx. $\text{Re} < 2100$) indicate

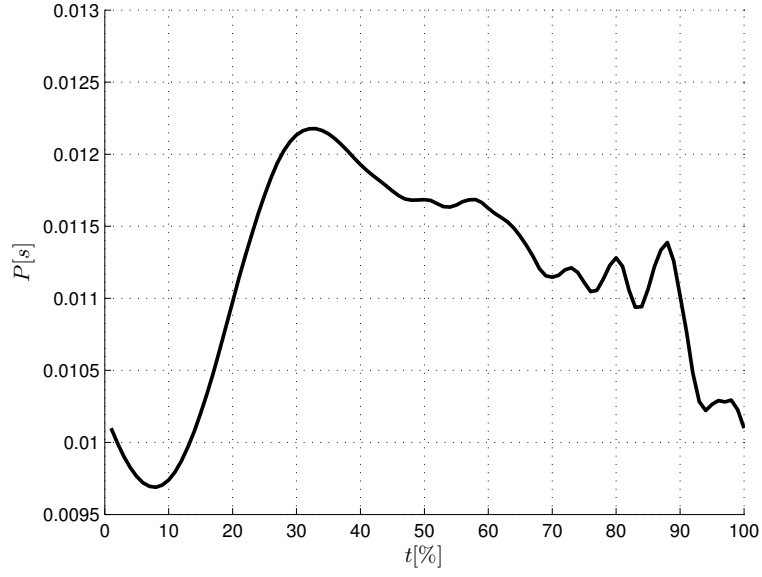


(a) Patient No. 3

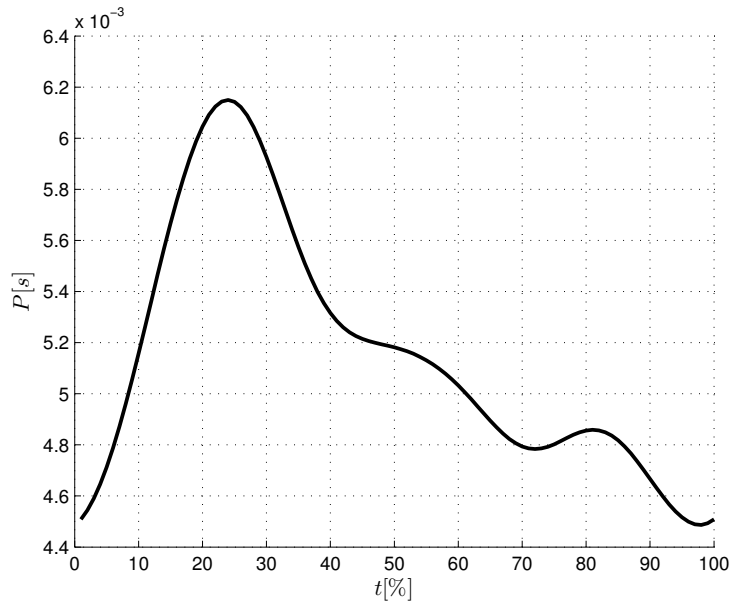


(b) Patient No. 5

Figure 2: Phase pictures. Local flow rate (cm^3/s) in time (s). Thick line – periodic solution, solid line – nullcline.



(a) Patient No. 3



(b) Patient No. 5

Figure 3: Sensitivity coefficient P (s) in time (% of the cardiac cycle).

laminar flow, while large values (approx. $Re > 4000$) correspond to turbulent
200 flow. In the transition zone, where also our example is situated, the behavior
strongly depends on the existing disturbances in the flow.

5. Discussion

Our work present a novel numerical algorithm for the non-invasive blood
flow quantification based on ECG-gated CT angiography images.

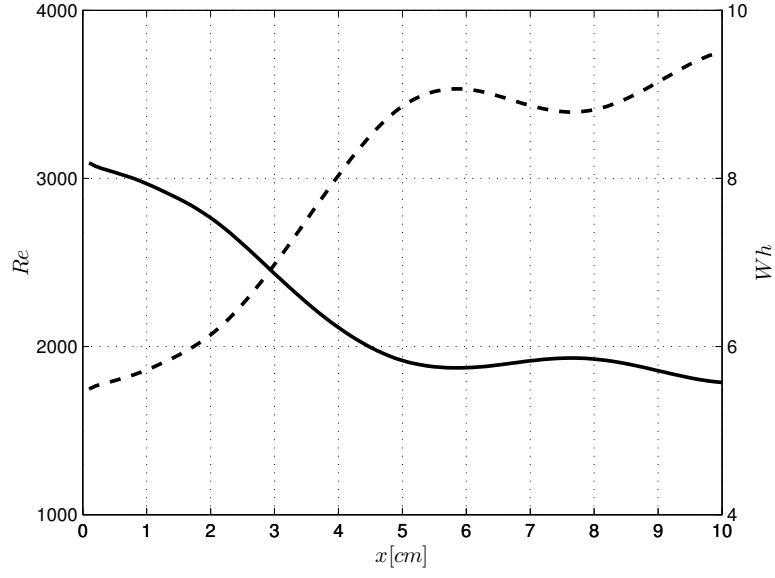
205 Quantification of flow in blood vessels provides important information aiding
the management of different clinical conditions [13]. Since its introduction in the
late 1980s, phase-contrast magnetic resonance (MR) imaging has become the
method of choice for flow quantification over ultrasound, as it is able to measure
time-resolved 3D flow with high accuracy and reproducibility without the need
210 of a good acoustic window [14]. Our approach enables us to calculate aortic
flow on a routine ECG-gated CT angiography dataset. This is of huge clinical
potential, as the knowledge of hemodynamic parameters could vastly improve
the diagnostic performance of CT imaging in several cardiovascular pathologies,
such as aortic coarctation or dissection. Our method can also be beneficial in
215 the management of patients who are not candidates for an MR examination
with long acquisition time either because of claustrophobia or due to unstable
patient status.

State-of-the-art investigations of the disorders of human arterial sections ap-
ply 3D numerical fluid-structure interaction simulations involving the calcula-
220 tion of the blood flow field inside the lumen, the necessary boundary conditions
of which are the time-dependent pressure profile at the outlet and volumetric
flow rate at the inlet cross-section. The protocol to determine these functions
non-invasively is the measurement of both on the arm followed by transforming
them to the section under scrutiny by a 1D systemal model of the circulatory
225 system. Our method offers a different and easy to use procedure to formulate
the inlet boundary condition without Doppler velocimetry, thus facilitating 3D
simulations.

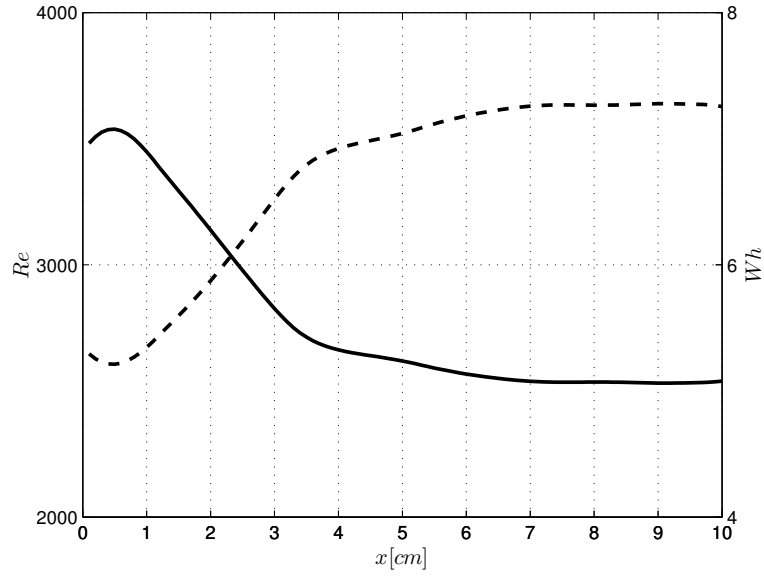
6. Conclusions

We presented a novel numerical algorithm for the non-invasive quantifica-
230 tion of blood flow based on ECG-gated CT angiography images. This method
can vastly improve the diagnostic performance of CT imaging in several cardio-
vascular pathologies. Further studies are needed to validate our approach in a
clinical setting.

A block-based optimization algorithm was developed to compute local flow
235 rate in time. The shapes of the local flow rate curves seem to be very similar
to the triphasic arterial curves that can be measured by invasive intraarterial
method. The mean squared error (MSE) values, which measures the goodness
of the model, are quite small compared to the average flow rate.



(a) Patient No. 3



(b) Patient No. 5

Figure 4: Reynolds and Whomersley numbers vs. distance from the beginning of the aorta segment (cm).

According to the analysis of Reynolds and Womersley numbers, the velocity profile has a complex time-dependent behaviour in the detailed examples (Patient No. 3 and No. 5).

We have found that conditions of Kotin's theorem are satisfied in most of the cases and the physically admissible solution is not asymptotically stable in general. Further mathematical analysis of equation (7) is needed to find weaker sufficient conditions for the physical admissibility.

References

- [1] G. S. K. Yunlong Huo, Pulsatile blood flow in the entire coronary arterial tree: theory and experiment, *American Journal of Physiology - Heart and Circulatory Physiology* 291 (3) (2006) H1074–H1087. doi:10.1152/ajpheart.00200.2006.
- [2] R. G. Moloy Kumar Banerjee, A. Datta, Effect of pulsatile flow waveform and womersley number on the flow in stenosed arterial geometry, *ISRN Biomathematics* 2012 (11) (2012) 1–17. doi:10.5402/2012/853056.
- [3] S. P. S. Mir Golam Rabby, M. M. Molla, Pulsatile non-newtonian laminar blood flows through arterial double stenoses, *Journal of Fluids* 2014 (2014) 1–13. doi:10.1155/2014/757902.
- [4] D. T. Michael Kass, Andrew P. Witkin, Snakes: Active contour models, *International Journal of Computer Vision* 1 (4) (1988) 321–331. doi:10.1007/BF00133570.
- [5] U. J. S. M. F. R. Christoph R. Becker, Bernd M. Ohnesorge, Current development of cardiac imaging with multidetector-row ct, *European Journal of Radiology* 36 (2) (2000) 97–103. doi:10.1016/S0720-048X(00)00272-2.
- [6] B. A. U. C. A. C. J. L. L. R. S. J. C. C. M. J. H. J. H. L. James P. Earls, Elise L. Berman, Prospectively gated transverse coronary ct angiography versus retrospectively gated helical technique: Improved image quality and reduced radiation dose, *Radiology* 246 (3) (2008) 742–753. doi:10.1148/radiol.2463070989.
- [7] V. H. Milan Sonka, R. Boyle, *Image Processing, Analysis, and Machine Vision*, Cengage Learning, 2008, iISBN-10: 1133593607.
- [8] J. K. Tomáš Svoboda, V. Hlaváč, *Image Processing, Analysis & Machine Vision - A MATLAB Companion*, Thomson Learning, 2007, iISBN: 0495295957.
- [9] R. Nagy, C. Csobay-Novák, A. Lovas, P. Sótónyi, I. Bojtár, Non-invasive in vivo time-dependent strain measurement method in human abdominal aortic aneurysms: Towards a novel approach to rupture risk estimation, *Journal of biomechanics* 48 (10) (2015) 1876–1886. doi:doi:10.1016/j.jbiomech.2015.04.030.

- 280 [10] L. Kotin, On positive and periodic solutions of riccati equations, SIAM Journal of Applied Mathematics 16 (6) (1968) 1227–1231. doi:10.1137/0116103.
- [11] K. K. C. M. C. Y. L. H. C. S. L. S. K. D. Jung JM, Lee DH, Reference intervals for whole blood viscosity using the analytical performance-evaluated scanning capillary tube viscometer., Clinical Biochemistry 47 (6) (2014) 489–93. doi:10.1016/j.clinbiochem.2014.01.021.
- 285 [12] G. J. Hinghofer-Szalkay H, Continuous monitoring of blood volume changes in humans., J. Appl. Physiol. (1985) 63 (3) (1987) 1003–7.
- [13] T. C. T. G. A.J. Powell, S.E. Maier, Phase-velocity cine magnetic resonance imaging measurement of pulsatile blood flow in children and young adults: In vitro and in vivo validation, Pediatric Cardiology 21 (2000) 104–110. doi:10.1007/s002469910014.
- 290 [14] J. G. K. B. J. Zoran Stankovic, Bradley D. Allen, M. Marki, 4d flow imaging with mri, Cardiovascular Diagnosis & Therapy 4 (2) (2014) 173–192. doi:10.3978/j.issn.2223-3652.2014.01.02.